

1 **Study on the influence of topography on wind shear-**
2 **numerical simulation based on WRF-CALMET**

3 Xingyu Wang¹, Yuhong Lei¹, Baolong Shi¹, Zhiyi Wang¹, Xu Li¹, Jinyan Wang¹

4 ¹Key Laboratory of Climate Resource Development and Disaster Prevention in
5 Gansu Province, College of Atmospheric Sciences, Lanzhou University, Lanzhou
6 730000, China

7 **Correspondence:** Jinyan Wang (wangjny@lzu.edu.cn)

8 **Abstract**

9 This study focuses on the critical issue of low-altitude wind shear, vital for
10 aircraft safety during takeoff and landing. Using the WRF-CALMET model, we assess
11 the impact of topography on low-level wind shear at Zhongchuan Airport. CALMET
12 outperforms WRF, showing improved simulation accuracy. CALMET's simulation
13 highlights diurnal variations in vertical wind shear, especially pronounced from
14 13:00 to 24:00. Notably, CALMET indicates 1-2 hazard levels higher wind shear for
15 aircraft operations compared to WRF in a significant area. Terrain sensitivity
16 experiments reveal CALMET's responsiveness to terrain changes during high wind
17 shear periods, with reduced impact at higher altitudes. CALMET's incorporation of
18 kinematic terrain influences, blocking effects, slope flow, and strengthened
19 diversion of near-surface airflow on complex terrain contribute to these
20 findings. This study confirms the efficacy of CALMET in simulating low-altitude wind
21 shear, emphasizing its superiority in capturing terrain influences and reducing the
22 aviation safety threat posed by low-altitude wind shear.

23 **Keywords** — wind shear; wind field-numerical simulation; airport; CALMET;
24 aeronautical meteorology; topographic effect

25 **1. Introduction**

26 According to the definition of the International Civil Aviation Organization
27 (ICAO), low-level windshear refers to the sharp change of spatial wind speed or
28 direction within a 600-meter altitude range. Wind shear includes both vertical and
29 horizontal components and typically occurs near fronts, coastlines and the surface.
30 In the process of taking off and landing, low-level wind shear will affect the airspeed
31 of the aircraft, causing great risks and even terrible accidents in serious cases
32 (Evans J, 1989). In June 1975, a Boeing 727 aircraft crashed during its landing at
33 Kennedy Airport due to encountering low-level wind shear, resulting in 113
34 fatalities and 11 injuries (Fujita T T, 1997); In June 2000, a Wuhan Airlines aircraft
35 crashed during landing, also due to encountering low-level wind shear. In 2017, a

36 New Zealand Airlines A320-200 aircraft experienced low-level wind shear during
37 landing, resulting in severe damage to the aircraft and significant economic losses.
38 Therefore, accurate simulation and prediction of low-level wind shear, especially on
39 complex terrain, is of great significance for ensuring the safety of aircraft takeoffs
40 and landings at airports.

41 However, achieving accurate predictions remains a primary challenge faced by
42 numerical weather forecasting models (Colman B.2012). Low-level wind shear is
43 influenced by multiscale weather systems and characterized by small temporal and
44 spatial scales, high intensity, and sudden occurrences, thus making it difficult to
45 detect, study and predict. In simulating actual wind fields, simple characteristics are
46 insufficient; the wind field structure around the airport must be included. There are
47 three main methods for calculating wind shear in model wind fields(Zhang
48 Y,2022):1.Using meteorological radar networks and various monitoring networks
49 around airports, differential methods are employed to collect measured data,
50 recording wind speed, and wind direction in a grid format. However, these
51 measurements are scattered and small, insufficient to capture the essential
52 characteristics and dynamic development of low-level wind shear, and do not vary
53 with meteorological conditions.2.The second type of wind shear model is common
54 in engineering and consists of simple models. These typically comprise some
55 physical concepts, represented through simple mathematical fitting and basic fluid
56 dynamics solutions. They only reflect essential features of the shear wind field
57 without fully capturing the true wind field characteristics(Li Hai,2016).3.The third
58 type of wind shear model is based on atmospheric dynamics and physical equations,
59 solved directly by large computers. Among these methods, the third not only
60 simulates the real wind shear in the wind field but also provides other useful
61 physical quantities (e.g., temperature, water content, and radar reflectivity),
62 revealing the formation process, causes, and development of wind shear. Many
63 studies have utilized numerical models to simulate low-level wind shear.

64 Boilley used the non-hydrostatic Meso-NH model to simulate two different
65 wind shear events in the complex terrain around Nice Côte d'Azur Airport. They
66 successfully predicted vertical wind shear and local turbulence; however, due to the
67 model resolution limitation (500m), the study did not accurately predict the time
68 and location of low-level wind shear. Consequently, subsequent wind shear studies
69 have continuously improved spatial resolution. The Weather Research and
70 Forecasting (WRF) model, designed for high-resolution mesoscale weather
71 forecasting, simulates airflow under realistic atmospheric conditions. However, due
72 to the grid resolution of WRF being greater than 1 km, it struggles to simulate the
73 small-scale airflow movements in complex terrain.Hong Kong International Airport
74 previously attempted to predict wind shear using the WRF model, affirming its
75 capability to forecast wind shear induced by terrain changes several hours in
76 advance and studied the model's performance under non-temperature inversion
77 conditions, it reproduced wind shear characteristics well. However, providing
78 precise warnings for the airport proved challenging(Chan PW.2016).Building on this,
79 Hong Kong International Airport conducted further research: using a 200m

80 resolution numerical weather prediction model, AVM, designed for fine short-term
81 weather forecasting based on WRF3.4.1 and during the whole research period, the
82 results consistent with the model forecast were observed on both runways(Hon K
83 K.2020). Since then, Hong Kong International Airport improved the WRF-based
84 coupled model, utilizing the WRF-LES coupled model to capture many wind
85 characteristics and micro-scale airflow within the airport, accurately reproducing
86 real wind direction changes (Chen F.2022). These studies demonstrate the
87 effectiveness of numerical models in simulating low-level wind shear in airport
88 regions, with higher resolution models providing better simulation results. The
89 series of studies conducted at Hong Kong International Airport suggests that
90 improving models based on the WRF model or coupling it with other models is a
91 promising approach for studying low-level wind shear. In previous studies, the
92 WRF/CALMET coupled model has never been used to study low-level wind shear in
93 airport regions. This study uses this model, significantly improving simulation
94 resolution and leveraging CALMET's advantages in wind field calculations,
95 providing a new method for numerical simulation of low-level wind shear in airport
96 areas.

97 Lanzhou Zhongchuan International Airport stands as one of the largest aviation
98 hubs in Northwest China, situated in the southeastern part of the Qinwangchuan
99 alluvial-fan basin, surrounded by mountains on all sides. The region is known for
100 frequent wind shear occurrences, a phenomenon that has become increasingly
101 common at Lanzhou Zhongchuan Airport due to the rapid growth in the number of
102 flights. Most wind shear events occur during spring and summer, particularly in May,
103 June, and July (Li L.2020). Statistical reports on wind shear at Lanzhou Zhongchuan
104 Airport indicate that the majority of incidents occur in the afternoon and evening.
105 This trend is attributed to the downward momentum in the afternoon, enhanced
106 convective activity from increased ground heating, and higher wind speeds. Severe
107 convective weather is more likely to occur in the late afternoon to evening,
108 contributing to a higher frequency of reported low-level wind shear events.
109 Conversely, fewer flights operate during the night, accompanied by reduced
110 convective weather, resulting in relatively fewer reports of aircraft encountering
111 low-level wind shear (Dang B.2013). In May 2016, Zhongchuan Airport installed
112 coherent Doppler lidar near the runway to study the characteristics of low-level
113 wind shear and provide warnings (Li L.2020). Numerical simulation studies on
114 wind shear at Zhongchuan Airport have been ongoing. Jiang L. et al. selected a 6
115 km×6 km area near the runway at Zhongchuan Airport to establish a digital
116 elevation model of the terrain. They used FLUENT software for numerical
117 simulation, solving iterative calculations to obtain the distribution characteristics of
118 wind speed and pressure in the simulated area (Jiang Lihui.2018). However,
119 FLUENT, being a Computational Fluid Dynamics (CFD) simulation software widely
120 used in engineering, science, and research fields, only considers the local turbulence
121 of terrain and buildings on the flow field. It does not account for factors such as
122 gravity and heat exchange in real atmospheric conditions. Therefore, relying solely
123 on FLUENT for simulating and warning wind shear at Zhongchuan Airport has its

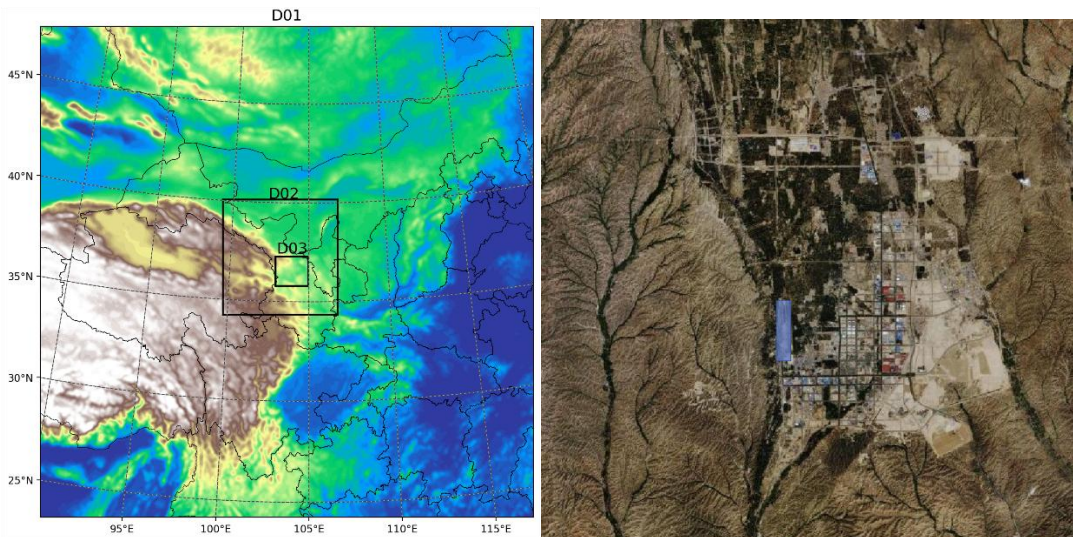
124 limitations. Improvements in simulating low-level wind shear still require
125 enhancements built upon numerical weather forecasting models.

126 In both domestic and international research, the CALMET model is frequently
127 employed to downscale WRF, providing a finer representation of microscale terrain
128 structures. Particularly in weak wind conditions, the CALMET downscaling coupling
129 model outperforms WRF in simulating near-surface wind directions(Zhang D.2020).
130 The WRF/CALMET coupled system demonstrates satisfactory performance in
131 various challenging scenarios, including the complex terrain of the Qinghai-Tibet
132 Plateau(Liao R.2021) and the intense weather system of Super Typhoon Meranti
133 (2016)(Tang S.2021). Up to now, no one has used WRF/CALMET coupling system to
134 simulate and test the occurrence of low-altitude wind shear. Therefore, this study
135 leveraged the dynamic downscaling effect of the CALMET model on local micro-
136 terrain to achieve high-resolution wind shear simulations with relatively low
137 computational requirements within a small area. Additionally, we conducted
138 controlled variable experiments by modifying the original terrain. This approach
139 has not been attempted in studies investigating terrain-induced wind shear at other
140 airports. It provides an improved method for simulating low-level wind shear
141 within the WRF model.

142 **2. Mode, Data, Method and Experimental Setup**

143 2.1 Models and Experimental Setup

144 In this study, the WRF model (version 4.2) was employed to simulate a severe
145 convective weather event occurring in the vicinity of Zhongchuan Airport over a
146 duration of 96 hours, starting from July 2, 2022, at 0000 UTC. The simulated wind
147 field results were then downscaled to 100 meters through coupling with the
148 CALMET model. The model utilized a three-layer, two-way nested domain
149 configuration (Figure 1a), with horizontal grid spacings of 9 km, 3 km, and 1 km. In
150 the vertical direction, there were 39 complete Eta layers from the surface to 0 hPa.
151 The physical schemes employed by WRF are detailed in Table 1.



153 (a) (b)

154 Figure 1. Three-layer Nested Domains of the WRF Model (a) and Simulation Area of
155 the CALMET Model © Google Maps(b), with the Zhongchuan Airport Highlighted in
156 Blue

157 Table 1. Model Configuration

Physical Scheme	WRF Option
Microphysics	Thompson graupel scheme (2-moment scheme in V3.1)
Cumulus parameterization	Tiedtke scheme
Longwave radiation	RRTMG
Shortwave radiation	RRTMG
Surface layer	Monin-Obukhov (Janjic Eta) scheme
Land surface	Noah
Boundary layer	MYJ

158 The diagnostic model utilized in this research is the CALMET model (version
159 6.5), which constitutes the meteorological component of the California Puff
160 Dispersion Model (Scire J S.2000). In the configuration of this study, the initial
161 guessed wind field is obtained from the grid wind field generated by the innermost
162 domain of WRF, with a horizontal grid spacing of 1 km (D3 in Figure 1(a)). Since no
163 objective analysis procedure is employed, we only pay attention to the first step
164 wind field. The coverage area of the CALMET model encompasses Zhongchuan
165 Airport and its surrounding 38km×38km region (Figure 1(b)), with a horizontal
166 resolution of 100m. The vertical layers are set to 10 height levels within 600 m
167 from the ground (the height range influenced by low-level wind shear).168 Terrain Sensitivity Experiments for Demonstrating the Impact of Terrain on
169 Wind Shear Simulation in CALMET:170 (1) CALMET: CALMET model configured with default settings as described
171 earlier.172 (2) CALEMFT_FLAT: Modification in the TERREL terrain processing module
173 where the elevation of all grid points is adjusted to 2000 meters. This adjustment
174 facilitates CALMET simulation on a flat underlying surface.175 (3) CALEMFT_RAISE: Modification in the TERREL terrain processing module
176 where the elevation of grid points with an altitude exceeding 2050 meters is
177 increased by 1.5 times. This modification enables CALMET to simulate wind shear
178 over a more rugged terrain.179 These terrain sensitivity experiments are designed to showcase how variations
180 in terrain impact wind shear simulation within CALMET. The CALMET_FLAT
181 experiment simulates wind shear on a flat surface, while the CALMET_RAISE
182 experiment explores wind shear simulation over steeper terrain. The comparison of
183 results from these experiments with the default CALMET setting will provide
184 insights into the sensitivity of wind shear simulations to terrain variations.

185 2.2 data

186 The terrain data comes from the global 90 m digital elevation data set of Shuttle
187 Radar Topography (SRTM3 V4.1) of NASA, and the land use data comes from the
188 global land cover type data with 10m resolution of Pengcheng Laboratory
189 (<https://data-starcloudpcl.ac.cn/zh>) of Tsinghua University in 2017.

190 The horizontal resolution of the ECMWF Reanalysis v5 (ERA5) dataset is $0.25^\circ \times 0.25^\circ$, with a temporal resolution of 1 hour. This dataset is employed as both the
191 initial input and boundary fields for WRF model. Additionally, this study utilizes
192 ERA5 variables, specifically geopotential height and temperature, for analyzing
193 weather systems during periods of intense convection.
194

195 Observational data for ground-level 10m wind speed at Lanzhou Zhongchuan
196 Airport are sourced from historical wind speed records provided by the National
197 Oceanic and Atmospheric Administration (NOAA)
198 (<https://www.ncei.noaa.gov/maps/daily/>) with a temporal resolution of 1 hour.
199 The ground 10m wind speed data of WRF model, CALMET model and ERA5
200 reanalysis data are interpolated to the location of Zhongchuan Airport, and
201 compared with the observed data to verify the performance of the models.

202 2.3 method

203 To quantify the differences in 10m wind speed among the experiments, the
204 following statistical metrics are employed:

205 Index of agreement (IA):

$$206 \quad IA = 1 - \frac{\sum_{i=1}^N (P_i - O_i)^2}{\sum_{i=1}^N (|P_i - \bar{O}| + |O_i - \bar{O}|)^2} \quad (1)$$

207 Root-mean-squared error (RMSE):

$$209 \quad RMSE = \sqrt{\frac{1}{n} \sum_{i=1}^n (O_i - P_i)^2}. \quad (2)$$

210 Mean relative error (MRE):

$$211 \quad MRE = \frac{1}{n} \sum_{i=1}^n \frac{(P_i - O_i)}{O_i} \quad (3)$$

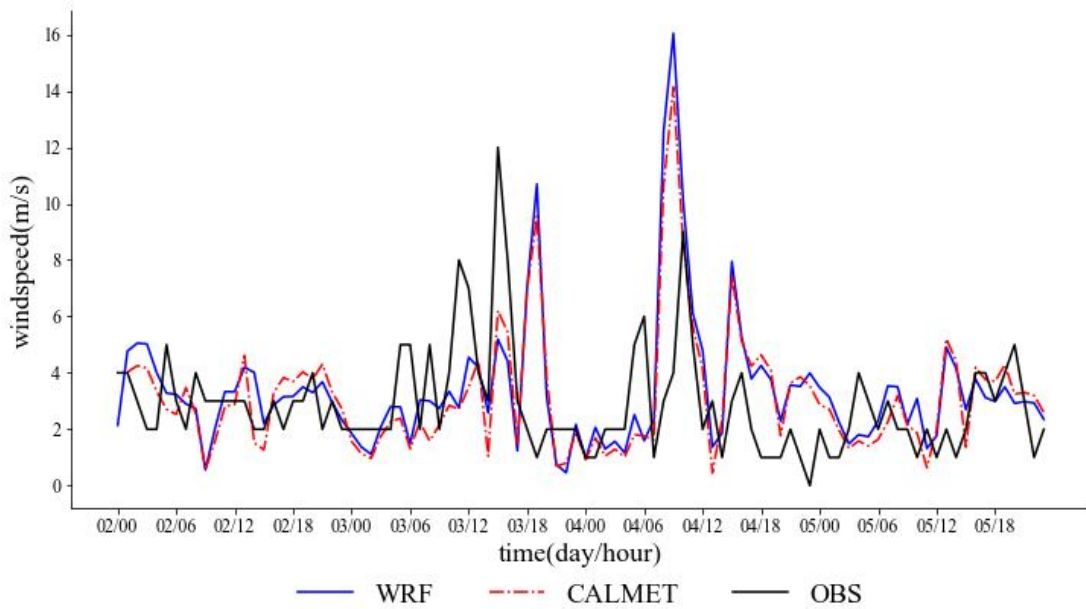
212 Here, \bar{O} and \bar{P} represent the average values of observational and simulated data,
213 respectively. Each observed value is denoted as O_i , and each simulated value is
214 denoted as P_i . Smaller values for MRE and RMSE, and an IA closer to 1.0, indicate
215 better simulation performance.

216 Wind shear can be categorized into three types: vertical shear β , meridional
217 horizontal shear α_1 , and zonal horizontal shear α_2 . Among these, vertical shear of
218 horizontal wind has a more significant impact on aircraft takeoff and landing
219 compared to the other types(Bretschneider, L.2022). It results in changes in wind
220 speed and direction as an aircraft moves through different altitudes, which can lead
221 to drastic changes in airflow during ascent or descent, thereby increasing flight
222 difficulty, particularly during takeoff and landing(Keohan, C.2007; Eggers, A.J.,
223 Jr.2003; Eggers, A.J., Jr.1992).

224 **3.Result**

225 3.1 Improvement of WRF/CALMET coupling model for simulation of low-level
226 wind shear.

227 We evaluated the performance of two models in simulating near-surface wind
228 speeds, as shown in Figure 2 and Table 2. Both models showed better agreement
229 with observed data during periods of low wind speeds before convective
230 development (06:00 on July 3) and after convective cessation (02:00 on July 5).
231 During periods of intense convection, both models captured wind speed variability.
232 Although both experiments underestimated or overestimated peak wind speeds on
233 July 3 and July 4, CALMET slightly outperformed WRF in simulating high wind
234 speeds. Furthermore, Table 2 indicates that CALMET's Mean Relative Error and
235 Root Mean Squared Error were lower than those of WRF throughout the entire
236 simulated period, with improvements of 11.13% and 7.24%, respectively. CALMET's
237 Index of Agreement was also closer to 1 compared to the WRF experiment, with an
238 improvement of 12.06%. These results demonstrate CALMET's superior overall
239 simulation performance compared to WRF.



240

Figure 2 :the time series of 10m surface wind speed for both numerical simulations and observational data

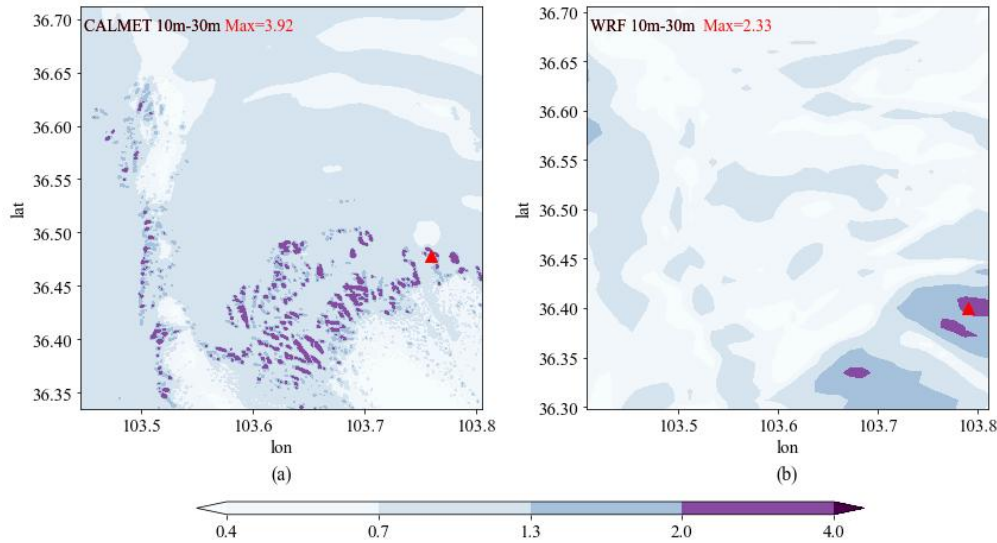
Table 2: Statistic results of near-surface wind speed simulations in different experiments averaged.

	WRF	CALMET	Improvement (%)
MRE (%)	43.255	38.425	11.13
RMSE(m /s)	2.713	2.517	7.24
IA	0.454	0.509	12.09

At 16:00 on July 3, significant fluctuations in surface wind speeds mark the onset of convective development (Figure 2). Figure 3 illustrates the distribution of Vertical Wind Shear (VWS) simulated by both models. In the layer between 10m and 30m above ground level, CALMET's maximum VWS values, while consistent in location with WRF's, are notably higher. Terrain analysis reveals CALMET simulates high VWS values near mountain foothills and western slopes (Figure 8). WRF's high VWS values primarily occur in mountainous regions. Details for the height layers of 200m-300m and 500m-600m can be found in the appendix. Overall, both models exhibit decreasing VWS with increasing height. From the overall distribution of VWS, CALMET can simulate a wider range of third and fourth level wind shears, which are associated with severe and extreme turbulence affecting aircraft takeoff and landing. Furthermore, this capability provides valuable warnings for aircraft operations at Nakawa Airport.

The atmosphere above and surrounding the mountainous terrain is characterized by three distinct regions or inclined layers, comprising the thermal structure undergoing diurnal variations and forming diurnal winds: slope atmosphere, valley atmosphere, and mountain atmosphere(Zardi, D.2013). It is challenging to observe any pure form of diurnal mountain wind system, as each component interacts with the others. Well-organized thermally driven flows can be identified over a broad spatial scale, ranging from the dimensions of the largest mountain ranges to the smallest local topography. Therefore, concerning wind shear in mountainous and foothill areas, wind shear in mountainous areas tends to be smaller. When airflow passes through mountain ridges, the lower-level airflow experiences significant compression. According to the conservation of flux, the acceleration effect on lower-level airflow exceeds that on upper-level airflow, resulting in an overall reduction in wind shear. When the acceleration effect on lower-level airflow is significant while the upper-level acceleration effect is weak or absent, negative wind shear occurs. Overall, the intensity of low-level wind shear may be greater near mountain foothills or ridges and lesser in valleys or slopes.

276 Hence, the regions of maximum wind shear simulated by CALMET near mountain
277 foothills or ridges are more consistent with reality than those by WRF.



278

279 Figure 3: Vertical Wind Shear (VWS) at 16:00 on July 3, 2022, simulated by
280 CALMET (a) and WRF (b) (Unit: m/s/10m). Triangles indicate the locations of
281 maximum values.

282 Figure 4 presents the time series of maximum VWS simulated by WRF and
283 CALMET. It can be observed that both WRF and CALMET simulations exhibit a clear
284 diurnal pattern in maximum VWS: maximum values are relatively small around
285 dawn and in the morning (1:00 to 12:00), with minimal fluctuations, while they
286 increase significantly in the afternoon and evening (13:00 to 24:00), showing larger
287 variations. However, the maximum values simulated by WRF are generally lower
288 than those by CALMET, with this difference being more pronounced in the afternoon
289 and evening. On July 3rd and 4th, during periods of intense convective activity,
290 CALMET is able to simulate larger fluctuations in maximum VWS compared to
291 normal conditions.

292 In summary, utilizing CALMET for downscaling WRF output of wind fields
293 provides higher resolution and more precise surface conditions, which are
294 advantageous for simulating mesoscale wind shear. This is primarily manifested in
295 the following aspects: the distribution of VWS in the mid-to-low levels is more
296 significantly influenced by terrain, and VWS decreases more rapidly with increasing
297 altitude; the diurnal variation of maximum VWS within VWS regions follows a clear
298 pattern and can reflect the characteristics of intense convection.

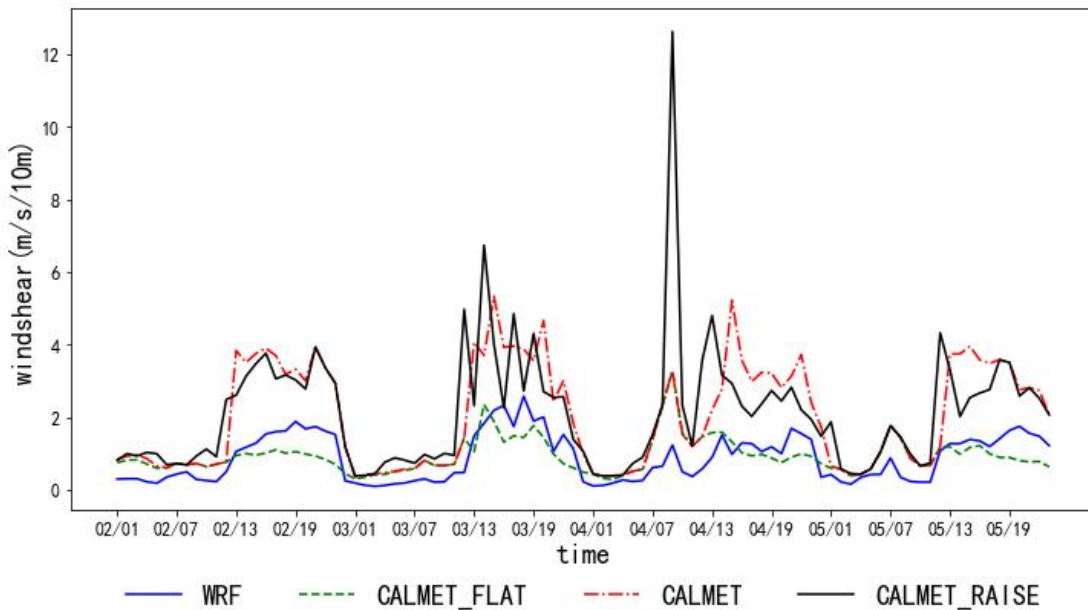
299 3.2 Impact of Topography on Wind Shear Simulation

300 Through different terrain configurations, we explored CALMET's detailed
301 terrain impact on low-level wind shear. We found that valley winds affect VWS
302 diurnal variation. Terrain, blocking effects, and slope flow kinematics enhance near-

303 surface airflow diversion, deflection, and ascent over complex terrain, significantly
304 influencing VWS, with the impact decreasing with height.

305 In the CALMET_FLAT experiment, the increase in maximum VWS during the
306 afternoon and evening is minimal (Figure 4), with slight fluctuations and values
307 around 2 m/s/10m, sometimes even lower than WRF. However, good agreement is
308 observed among the three experiments during the early morning and morning
309 periods. In CALMET_RAISE, particularly on July 3rd and 4th during intense
310 convective development, fluctuations in the afternoon and evening are more
311 pronounced compared to CALMET. However, CALMET_RAISE shows stability
312 similar to CALMET just before convective development on July 2nd, except for an
313 unusually high value at 09:00 on July 4th, where fluctuations are more pronounced,
314 but numerically close to CALMET.

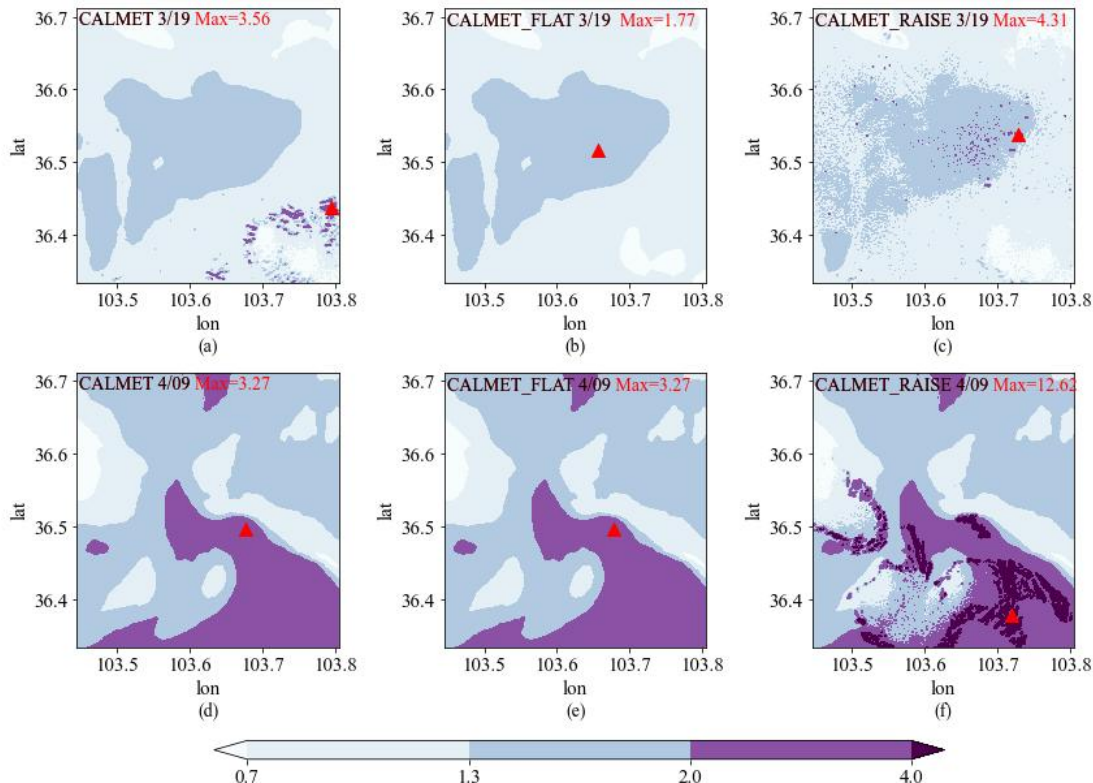
315 In the afternoon and evening, CALMET_FLAT shows a significant decrease in
316 maximum VWS, while CALMET_RAISE exhibits more pronounced fluctuations. For
317 example, at 19:00 on July 3rd (Figure 5(a)-(c)), in the CALMET experiment, the
318 maximum VWS (3.56 m/s/10m) occurs in the southeastern foothills and valley
319 areas. In CALMET_FLAT, except for the absence of a high-value area in the southeast,
320 the distribution is similar to CALMET, with a maximum value of 1.77 m/s/10m in
321 the central region, which is also a flat valley area in CALMET. In CALMET_RAISE,
322 due to a sudden 1.5-fold increase in terrain elevation above 2050m, the steep terrain
323 causes chaotic wind shear distribution, with scattered high values in the central
324 region, and the maximum value increases to 4.31 m/s/10m. In summary,
325 transitioning from complex to flat terrain shifts the location of maximum VWS from
326 mountainous areas to flat valleys.



327

Figure 4: Time series of 10m-30m maximum VWS values of different simulation experiments in the study area

330 This phenomenon is a typical result of valley winds, driven by the interaction
331 between terrain and solar radiation. During the day, sunlight heats the surface,
332 leading to differential heating rates between slopes and valleys due to their distinct
333 topographies. Slopes, receiving direct sunlight, warm up faster than valleys. At night,
334 the surface loses heat, particularly in valleys with good heat dissipation, resulting in
335 strong nighttime cooling effects. The temperature difference between slopes and
336 valleys during the day induces upslope airflow along the slopes. As the heated air
337 ascends, airflow forms over the valleys, as depicted in Figure 5(a) where maximum
338 VWS occurs near mountainous areas. At night, cold air flows downhill along the
339 slopes, forming downslope winds, which reverse the airflow pattern observed
340 during the day.



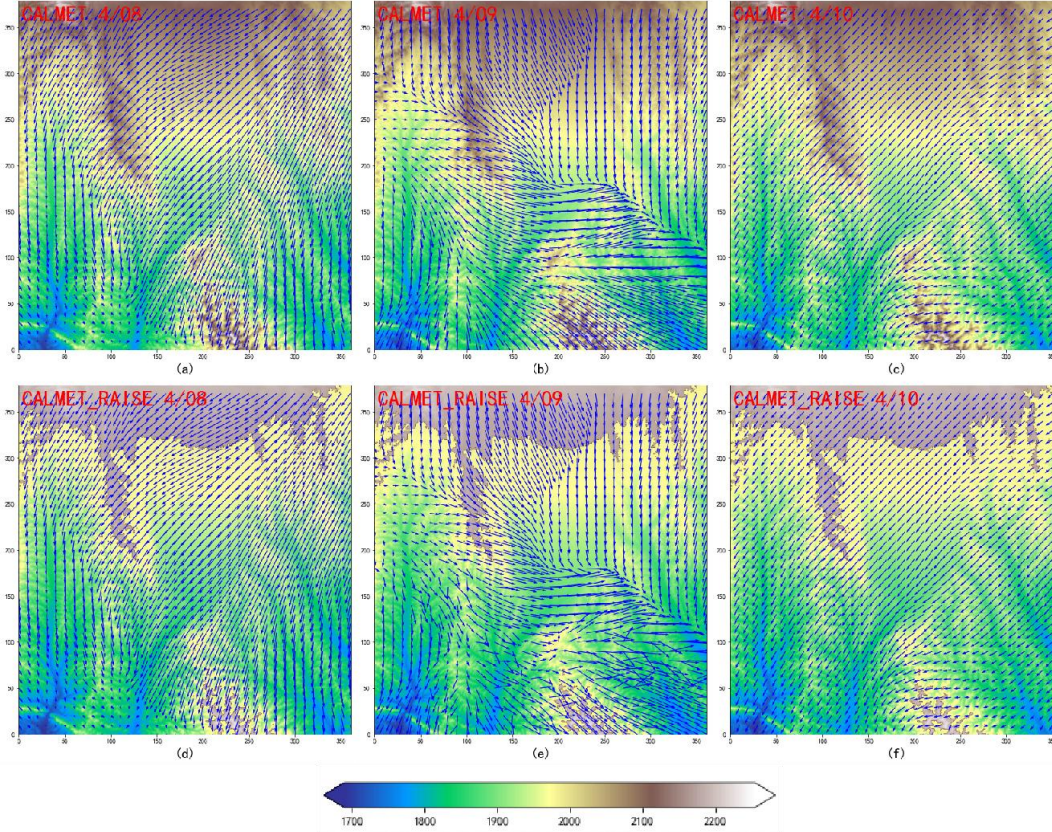
342 Figure 5: VWS distribution of 10m-30m.(a)-(c): 19:00 on July 3, 2022; (d)-(f):
 343 09:00 on 4 July 2022; (a),(d):CALMET; (b),(e):CALMET FLAT; (c),(f):CALMET RAISE.

344 The results indicate that CALMET model simulations of VWS are highly
345 sensitive to terrain: VWS values are generally lower in flat terrain compared to
346 complex terrain, and the influence of terrain on wind shear diminishes rapidly with
347 height. In extremely steep terrain, near-surface distribution appears chaotic, but
348 VWS values notably increase above the surface compared to complex terrain. Across
349 the three experiments, the absolute differences in VWS decrease with height,

350 suggesting a diminishing impact of terrain on CALMET model simulations of VWS
351 with increasing altitude.

352 To investigate extreme high values of VWS in the CALMET_RAISE experiment at
353 09:00 on July 4th, Figures 5(d)-(f) display the VWS distribution for all experiments
354 at this time, while Figure 6 presents wind vector maps for three hours for both
355 CALEMT and CALEMT_RAISE. The VWS distribution for CALEMT and CALEMT_FLAT
356 is similar, with a peak of 3.27m/s/10m in the central region. Compared to July 3rd
357 at 19:00, both experiments show extensive high-value areas in the southeast, with
358 CALMET_RAISE reaching an exceptional maximum of 12.62m/s/10m in the
359 southeastern valley area. Additionally, CALMET_RAISE exhibits large areas of
360 exceptionally high values compared to the other experiments.

361 In Figure 6, at 08:00 and 10:00 on July 4th, the prevailing wind direction in the
362 area is northeast. Both CALMET and CALEMT_RAISE show similar wind field
363 structures, transitioning from northeast to north as terrain slopes southward. When
364 airflow passes through the southern valley, mountain ranges create denser wind
365 vectors and increased speeds. However, at 09:00, a strong northwest airflow
366 converges with the northern airflow, forming a distinct "micro-front." The terrain
367 blocking induces diversion, deflection, and upward motion of the northwesterly
368 wind, creating extensive high-value VWS areas in the southeast. Compared to
369 CALMET, CALEMT_RAISE exhibits a more chaotic wind field due to increased terrain.



370
 371 figure 6. Topographic Elevation (unit: m) and Wind Vector Distribution. (a)-(c)
 372 CALMET; (d)-(f) CALMET_RAISE; (a), (d) July 4th, 08:00; (b), (e) July 4th, 09:00; (c),
 373 (f) July 4th, 10:00.

374 In conclusion, the widespread high-value VWS area observed at 09:00 on July
 375 4th resulted from a shift in wind direction to the northwest, encountering minimal
 376 velocity reduction before reaching the tall terrain in the south, where the
 377 mountainous obstruction led to diversion, deflection, and upward motion. The
 378 anomalously high values in the CALEMNT_RAISE experiment were attributed to the
 379 elevation of the terrain, significantly intensifying the effects of diversion, deflection,
 380 and upward motion. This suggests that terrain has a more pronounced impact on
 381 CALMET-simulated wind shear during high wind speeds, while its influence is less
 382 evident during low wind speeds. Therefore, heightened awareness of low-level wind
 383 shear occurrence is warranted in complex terrain.

384 **4 Conclusion**

385 In order to investigate whether higher-resolution numerical models yield
 386 better simulation results for low-level wind shear, this study focuses on a severe
 387 convective weather event that occurred in the vicinity of Zhongchuan Airport on
 388 July 2, 2022. The WRF/CALEMNT coupled model is utilized to simulate the wind field,
 389 and the influence of terrain variations on CALMET-simulated wind shear is explored.
 390 The main conclusions are as follows:

391 (1) CALMET improves the simulation of near-surface winds, bringing them
392 closer to observed data than WRF, thereby facilitating more accurate modeling of
393 low-level wind shear.

394 (2) The diurnal variation of VWS shows a distinct pattern. CALMET exhibits
395 higher VWS compared to WRF, especially during the afternoon and evening. During
396 periods of intense convective activity, CALMET captures larger VWS fluctuations,
397 including higher peak values. CALMET's finer terrain features result in a VWS
398 distribution that better aligns with terrain effects, with VWS generally higher near
399 foothill areas compared to mountains, and a more pronounced decrease with
400 altitude.

401 (3) Terrain sensitivity experiments show that during early morning and
402 morning hours, the maximum VWS of the three experiments were similar, occurring
403 in flat regions with minimal terrain influence. However, in the afternoon and
404 evening, CALMET_FLAT shows decreased maximum VWS values, while
405 CALMET_RAISE exhibits drastic fluctuations, with peak values near mountainous
406 areas, indicating significant terrain influence. Moreover, the impact of terrain on
407 CALMET-simulated VWS diminishes with altitude. These findings highlight the
408 substantial influence of terrain on CALMET, particularly during periods of high wind
409 speeds.

410 (4) The occurrence of abnormally high VWS values in the simulations is
411 attributed to strong disturbances caused by tall terrain features: wind direction
412 shifts to northwest winds, encountering minimal reduction in wind speed before
413 encountering the tall terrain in the southern region. CALMET_RAISE elevates the
414 terrain from its original level, enhancing channeling, swirling, and updraft effects.

415 CALMET is a mature dynamic regional downscaling tool, and using other
416 numerical weather prediction models can also achieve the scale of CALMET. We
417 chose to use CALMET for the following reasons: from the perspective of operational
418 considerations, conducting research at the same scale requires lower computational
419 requirements and hardware needs for the CALMET model.

420 The research findings of this study are solely based on a short-term simulation
421 period of weather events in the Zhongchuan Airport area. However, this specific
422 case does not necessarily represent the overall wind shear situation at the airport,
423 as it is just one weather event with significant wind shear. And Obtaining radar wind
424 profiler data for the airport poses certain difficulties, we do not have Doppler lidar
425 equipment available. Direct observation of wind shear is challenging. We have made
426 efforts to obtain reanalysis data and site wind speed observations as much as
427 possible. Due to limited funding in the preliminary stages of our research, we could
428 only start with theoretical studies, and field experiments will be conducted once
429 funding becomes available. Our future work will expand to include longer simulation
430 periods in more airports and regions with complex terrain. This expansion aims to
431 examine and quantify the additional value provided by CALMET in simulating low-
432 level wind shear.

433

434 *Competing Interests.* The corresponding author declares that all authors have no
435 competing interests.

436 **Acknowledgment**

437 This work was supported by the Joint Funds of the National Natural Science
438 Foundation of China (Grant No. U2342205), the Gansu Provincial Association of
439 Science and Technology Innovation Drive Promotion Project (Grant No.
440 GXH20230817-7), and the Key Natural Science Foundation of Gansu Province (Grant
441 No. 23JRRA1030). We extend our sincere appreciation to the funding agencies for
442 their support.

443 Additionally, we would like to express our gratitude to the Supercomputing
444 Center of Lanzhou University for their assistance.

445

446 **References**

447 Boilley A, Mahfouf J F. Wind shear over the Nice Côte d'Azur airport: case studies[J].
448 Natural Hazards and Earth System Sciences, 2013, 13(9): 2223-2238.

449 Bretschneider, L.; Hankers, R.; Schönhals, S.; Heimann, J.-M.; Lampert, A. Wind Shear
450 of Low-Level Jets and Their Influence on Manned and Unmanned Fixed-Wing
451 Aircraft during Landing Approach. *Atmosphere* **2022**, *13*, 35.
452 <https://doi.org/10.3390/atmos13010035>

453 Chan PW, Hon KK (2016b) Observation and numerical simulation of terrain-Induced
454 windshear at the Hong Kong International Airport in a planetary boundary layer
455 without temperature inversions. *Adv Meteorol* Artic ID. <https://doi.org/10.1155/2016/1454513>

457 Chen F, Peng H, Chan P, et al. Identification and analysis of terrain-induced low-level
458 windshear at Hong Kong International Airport based on WRF-LES combining
459 method[J]. *Meteorology and Atmospheric Physics*, 2022, 134(4): 60.

460 Colman B, Cook K, Snyder B J. Numerical weather prediction and weather
461 forecasting in complex terrain[M]//Mountain Weather Research and Forecasting:
462 Recent Progress and Current Challenges. Dordrecht: Springer Netherlands, 2012:
463 655-692.

464 Dang, B., W. Z. Sun, J. Y. Wang, et al., 2013: Analysis of low-altitude wind shear cases
465 at Lanzhou Zhongchuan Airport during 2004–2007. *J. Lanzhou Univ. (Nat. Sci.)*, 49,
466 63–69, doi:10.3969/j.issn.0455-2059.2013.01.012. (in Chinese)

467 Eggers, A.J., Jr.; Digumarthi, R.; Chaney, K. Wind Shear and Turbulence Effects on
468 Rotor Fatigue and Load Control. *J. Sol. Energy Eng.* **2003**, *125*, 402–409.

469 Evans J, Turnbull D. Development of an automated windshear detection system
470 using Doppler weather radar[J]. Proceedings of the IEEE, 1989, 77(11): 1661-1673.

471 Fujita T T, Caracena F. An analysis of three weather-related aircraft accidents[J].
472 Bulletin of the American Meteorological Society, 1977, 58(11): 1164-1181.

473 Hon K K. Predicting low-level wind shear using 200-m-resolution NWP at the Hong
474 Kong International Airport[J]. Journal of Applied Meteorology and Climatology,
475 2020, 59(2): 193-206.

476 Jiang Lihui, Liu Xiaoyu, Li Zhen, et al. Study on the influence of terrain and buildings
477 around Lanzhou Zhongchuan Airport on wind field [J]. Computer and Digital
478 Engineering, 2018, 46(3): 561-565,626.

479 Keohan, C. Ground-based wind shear detection systems have become vital to safe
480 operations. *ICAO J.* **2007**, *62*, 16–19, 33–34.

481 Liao R, Fang X, Liu H, et al. Wind characteristic in the complex underlying terrain as
482 studied with CALMET system[C]//Journal of Physics: Conference Series. IOP
483 Publishing, 2021, 2006(1): 012053.

484 Li Hai, Zhou Meng, Guo Qinghua , Wu Renbiao , Xi Jiangtao. Compressive sensing-
485 based wind speed estimation for low-altitude wind-shear with airborne phased
486 array radar[J], Multidimensional Systems and Signal Processing,2016,7:1-14

487 Li L, Shao A, Zhang K, et al. Low-level wind shear characteristics and lidar-based
488 alerting at lanzhou zhongchuan international airport, China[J]. Journal of
489 Meteorological Research, 2020, 34(3): 633-645.

490 Roland, J. White Effect of wind shear on airspeed during airplane landing approach. *J.*
491 *Aircr.* **1992**, *29*, 237–242.

492 Scire J S, Robe F R, Fernau M E, et al. A user's guide for the CALMET Meteorological
493 Model[J]. Earth Tech, USA, 2000, 37.

494 Tang S, Huang S, Yu H, et al. Impact of horizontal resolution in CALMET on simulated
495 near-surface wind fields over complex terrain during Super Typhoon Meranti
496 (2016)[J]. Atmospheric Research, 2021, 247: 105223.

497 Zardi, D., Whiteman, C.D. (2013). Diurnal Mountain Wind Systems. In: Chow, F., De
498 Wekker, S., Snyder, B. (eds) Mountain Weather Research and Forecasting. Springer
499 Atmospheric Sciences. Springer, Dordrecht. https://doi.org/10.1007/978-94-007-4098-3_2

501 Zhang D, Chen L, Zhang F, et al. Numerical simulation of near-surface wind during a
502 severe wind event in a complex terrain by multisource data assimilation and
503 dynamic downscaling[J]. Advances in Meteorology, 2020, 2020: 1-14.

504 Zhang Y, Jia M. Low-level wind shear of wind field modeling and simulation[J]. 2022.